



# A Computational Pipeline for Prompt Gamma-Ray Burst Localization Aboard APT and ADAPT

Washington University in St. Louis

Ye Htet (htet.ye@wustl.edu), Marion Sudvar, Jeremy Buhler, Roger Chamberlain, James Buckley for the APT collaboration

Funded by NASA award 80NSSC21K1741 and NSF award CNS-1763503



1

## Overview

The Advanced Particle-Astrophysics Telescope (APT) [1,3] is a space-based mission concept for a combined gamma-ray and cosmic-ray observatory aimed at providing all-sky sensitivity, a very large effective area, and prompt localization of MeV transients such as GRBs. ADAPT (the Antarctic Demonstrator for APT) is under construction and scheduled to fly in late 2025. We are developing a low-latency computational pipeline for GRB localization fully onboard the instrument. Front-end preprocessing and event building stages are deployed on a set of FPGAs. Back-end CPU-based algorithms perform multi-Compton reconstruction and localization of the resulting Compton rings. **This poster describes:**

- An overview of the back-end algorithm for GRB localization
- An updated model, based on simulations and lab-based instrument measurements, of the detector and front-end that impacts uncertainty in the measured positions and deposited energies of Compton scatters in ADAPT
- An updated model of the anisotropic background radiation in the upper atmosphere and event pileup for ADAPT
- Experimental results of the localization accuracy with the updates in consideration including a new neural network approach
- Future work in progress: zero suppression, background suppression and neural network

2

## Background

### How We Localize GRBs

Gamma-ray photons from a GRB enter the instrument, interacting via one or more Compton scatters before being photoabsorbed. As described in [2], GRB localization occurs in two phases:

### (1) Reconstruction

- Infers time ordering of *one* photon's interactions w/ detector
- Photon reduces to *Compton ring* ( $c, \phi$ ), where  $c$  is vector through first two interactions and  $\phi$  is inferred angle between  $c$  and photon's source direction  $s$

### (2) Localization

- Intersects 100s to 1000s of Compton rings to infer common source direction  $s$  for GRB
  1. Produce rough guess at  $s$  by testing likelihood of candidate directions from small random sample of Compton rings
  2. Use iterative least-squares to refine estimate of  $s$  until convergence

### GRB Model

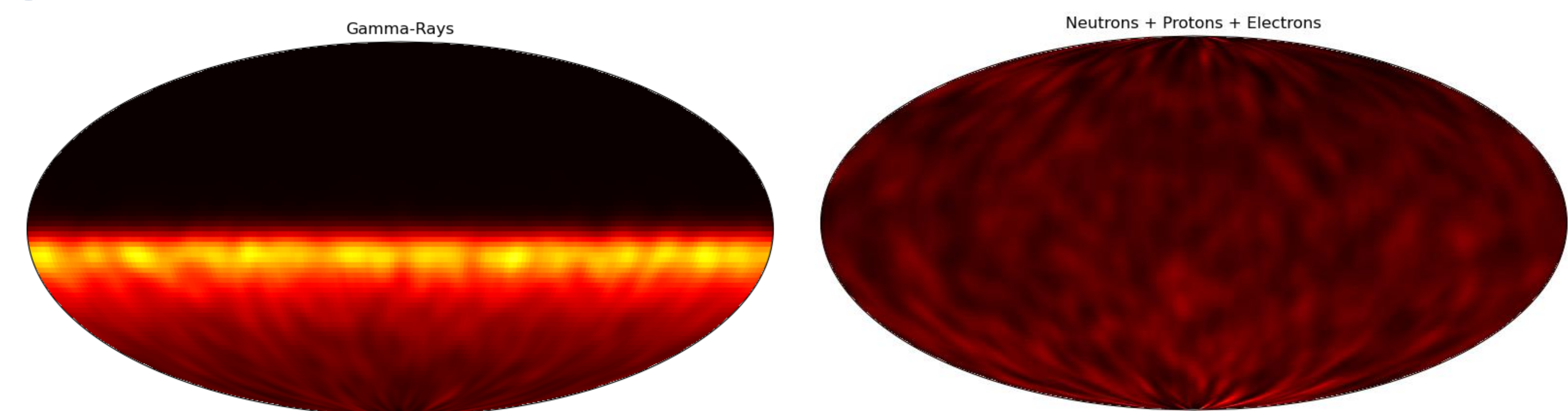
- Simulated bursts with Band spectra [8];  $\alpha = -0.5$ ,  $E_{\text{peak}} = 490$  keV,  $\beta = -2.35$
- Spectral energies in [30 keV-30 MeV] to approximately match sensitivity of Fermi GBM [9]
- Burst duration of one second, with time-intensity profile of [5, Sec. 5]
- Generated gamma rays, modeled interactions with detector using GEANT4 [4]

### Measuring GRB Localization Accuracy

- Infer source direction from GEANT4-simulated photons from model burst(s)
- Measure angular diff. between true, inferred source directions
- Over 1000 trials, report 68% ( $1\sigma$ ) and 95% ( $2\sigma$ ) *containment* values (i.e., 68/95% of trials yield at most given angular error)

4

## Atmospheric Particle Background and Pileup



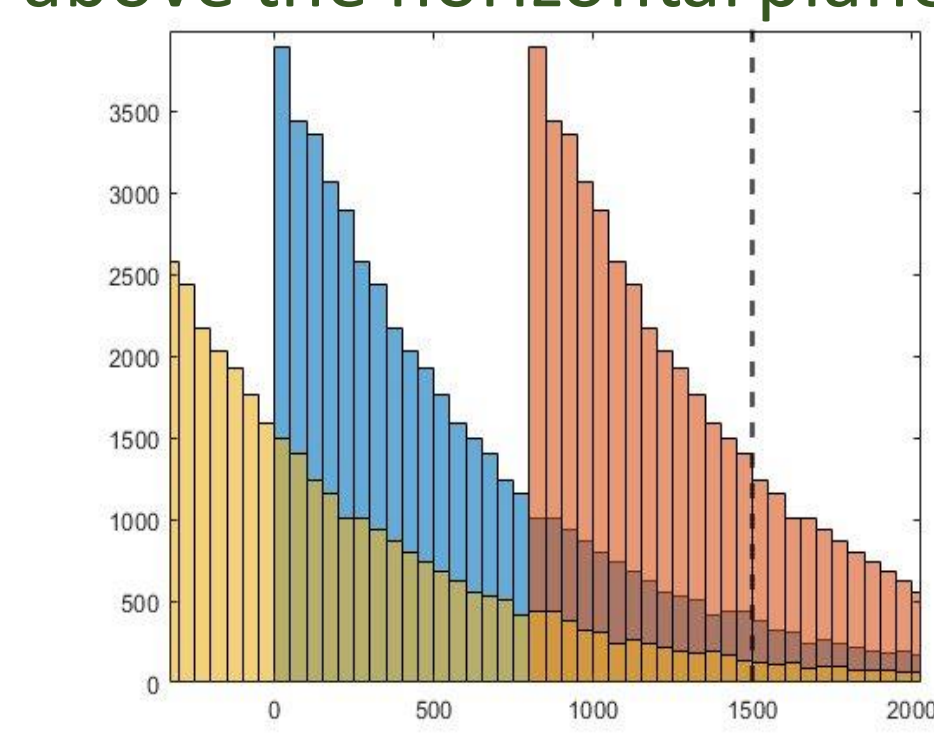
### Background Particles

In the Earth's upper atmosphere, ADAPT will be exposed to significant anisotropic background radiation from the Earth's limb. **Current Solution:**

- (1) Remove all events in which two or more interactions occur in the same layer
- (2) Rejects all the Compton ring lies entirely below the horizontal as GRBs can occur only above the horizontal plane for ADAPT

### Pileup

- Signals from multiple events may be captured within the same ALPHA readout window.
- Individual gamma-ray photon arrival times sampled from a normal distribution in the interval [0,1],  $\text{std}=0.25\text{s}$
- Events triggered by the anisotropic background radiation may also pile up



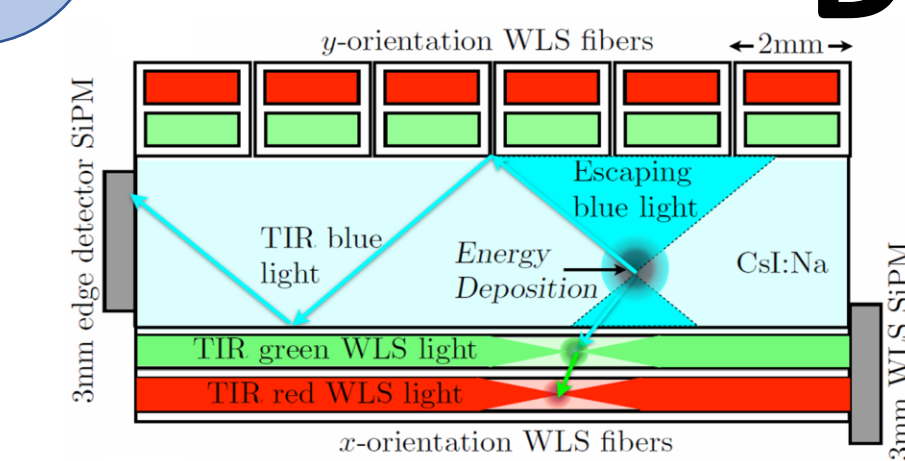
Containment	Background Complete	Background & Pileup Complete	Background & Pileup (ACD + BGO) Shielding	Background & Pileup (ACD + BGO) Shielding + NN
68% cnt.	6.89 ± 0.10	13.42 ± 0.43	4.56 ± 0.07	3.08 ± 0.07
95% cnt.	18.48 ± 0.03	56.76 ± 4.74	9.10 ± 0.22	7.25 ± 0.20

Using the complete background with pileup can greatly degrade our accuracies, we implemented shielding and also tested an initial Neural Network Model (Sec. 6)

- An anticoincidence detector (ACD) to avoid triggering on protons, neutrons, and electrons
- Active bismuth germanate (BGO) Compton-suppression shielding at the bottom
- Source / background Compton ring count: 136 / 26 (w/ shielding) vs 165 / 430 (w/o shielding)

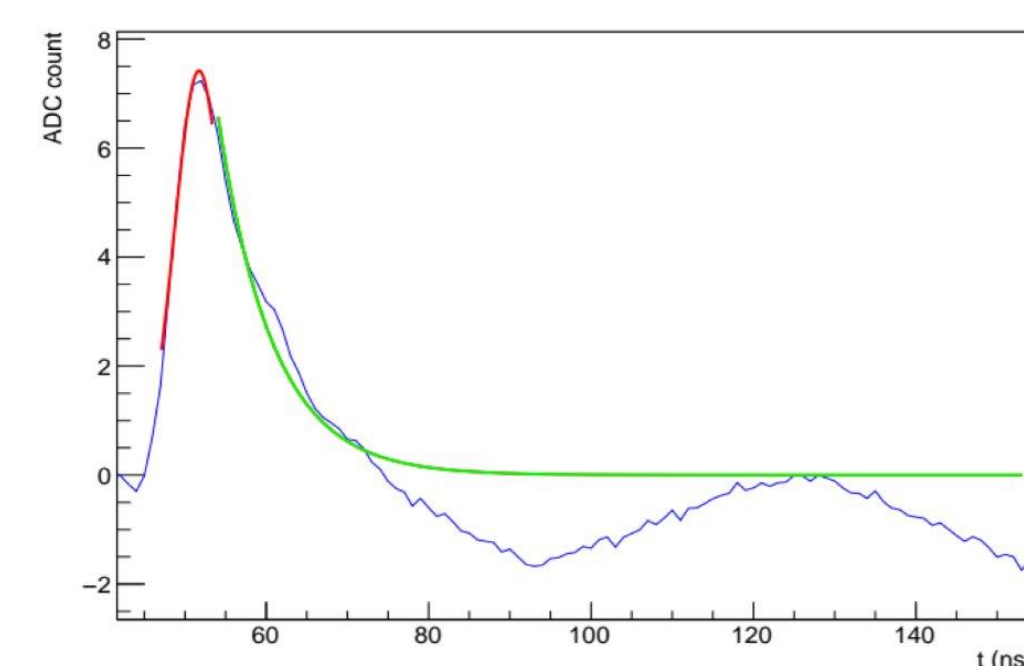
3

## Detector Noise Simulation



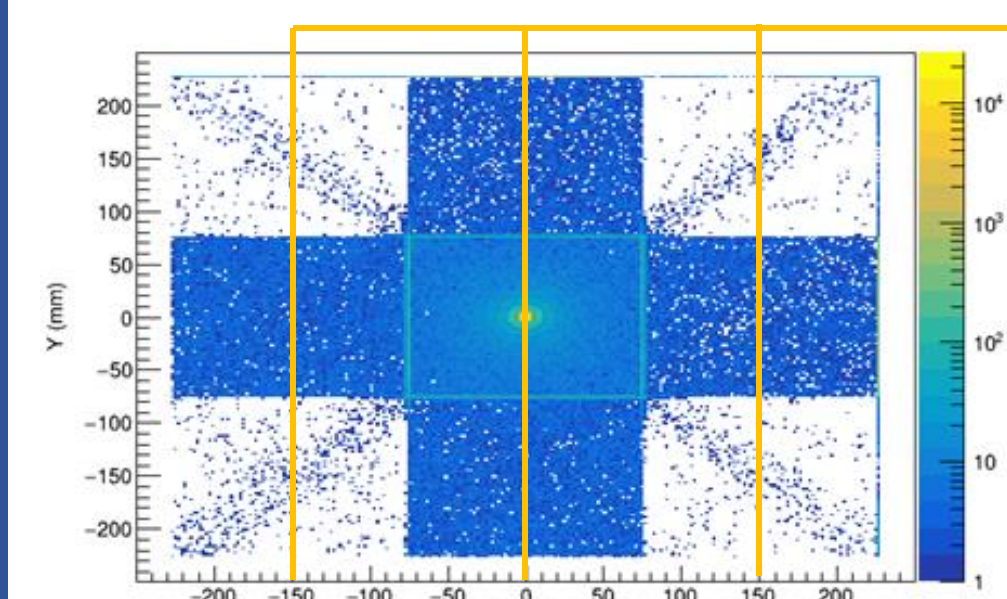
### Smart Preamplifier Noise

- RMS noise per ns:  $\sigma = 1.39$
- Further scale by signal integration time
- SMART single-PE impulse response modeled using 13ns Gaussian followed by 27ns exponential
- MC simulation determines mean and std for ADC count



### Edge Detector Modeling

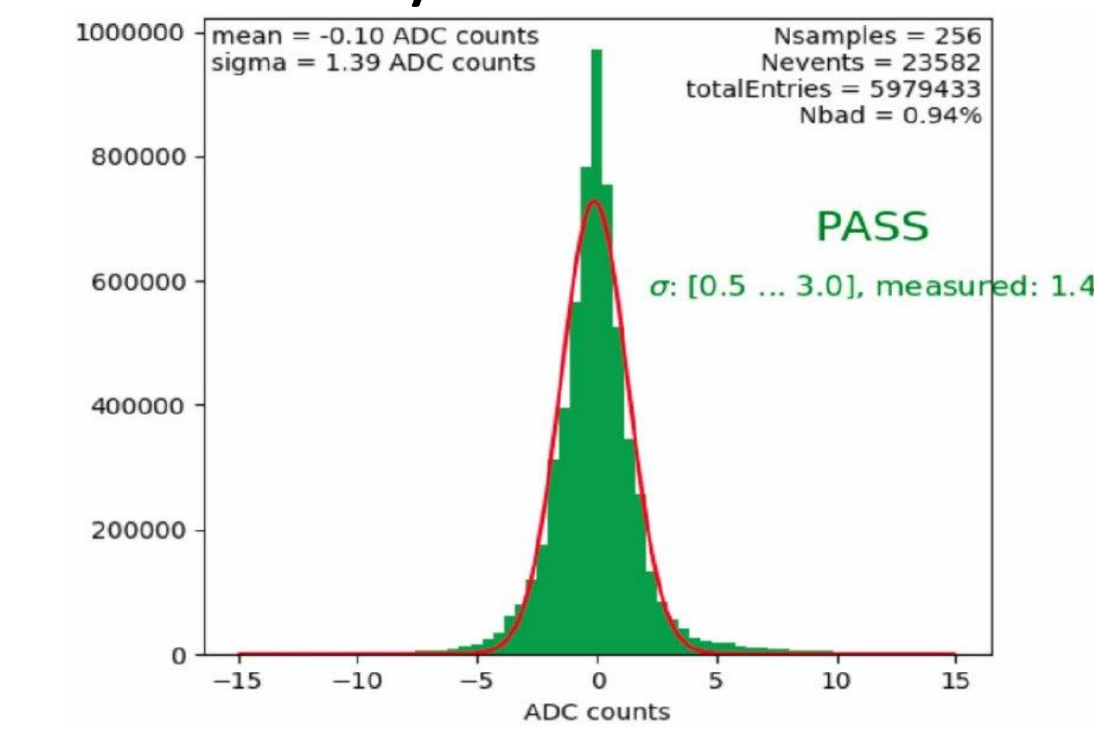
- Optical simulations of ICC layer provide distributions of scintillated photons detected by edge SiPMs
- Using the estimated x/y positions localized from the fibers, we can convert integrated signal amplitude to energy



Photon absorption positions from point-like energy deposit at center.

### SiPM Dark Counts

- Rel. overvoltage  $\sim 5\%$
- Cooled to  $10^\circ\text{C}$
- 70 kHz for single  $3 \times 3$  mm SiPM

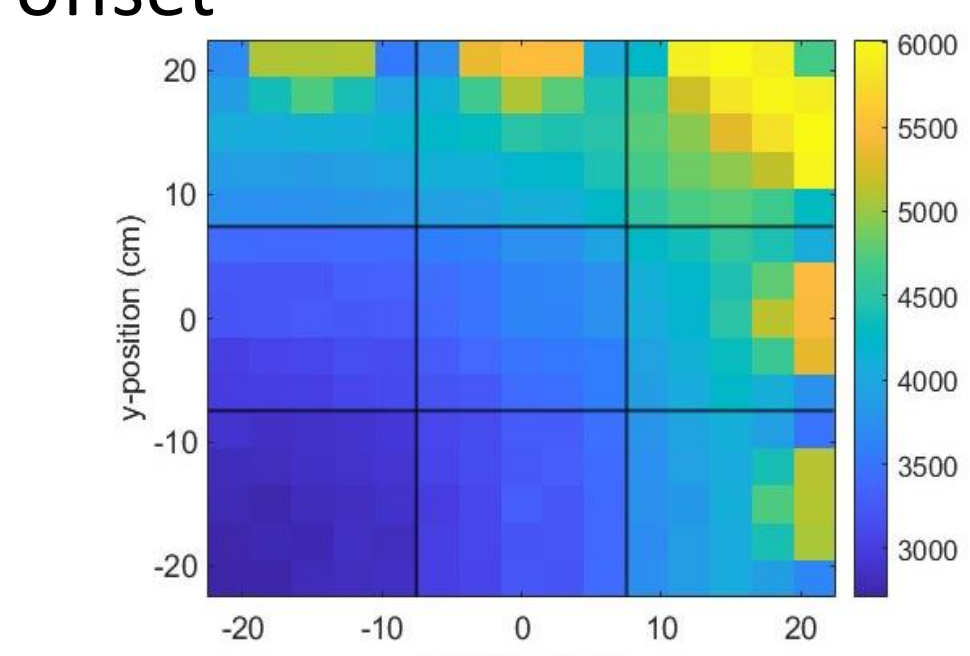


### Signal integration

- 10ns sampling by analog front-end digitizer ASICs
- CsI scintillation modeled as 633 ns exponential distribution
- $1 \mu\text{s}$  integration for edge detector and WLS fiber signals
- Integration window selected to trade off more optical photon capture and less noise (dark count and preamplifier RMS)

### WLS fiber transmission efficiency

- The WLS fiber transmission is fit to the lab measurements as an exponential with DC offset



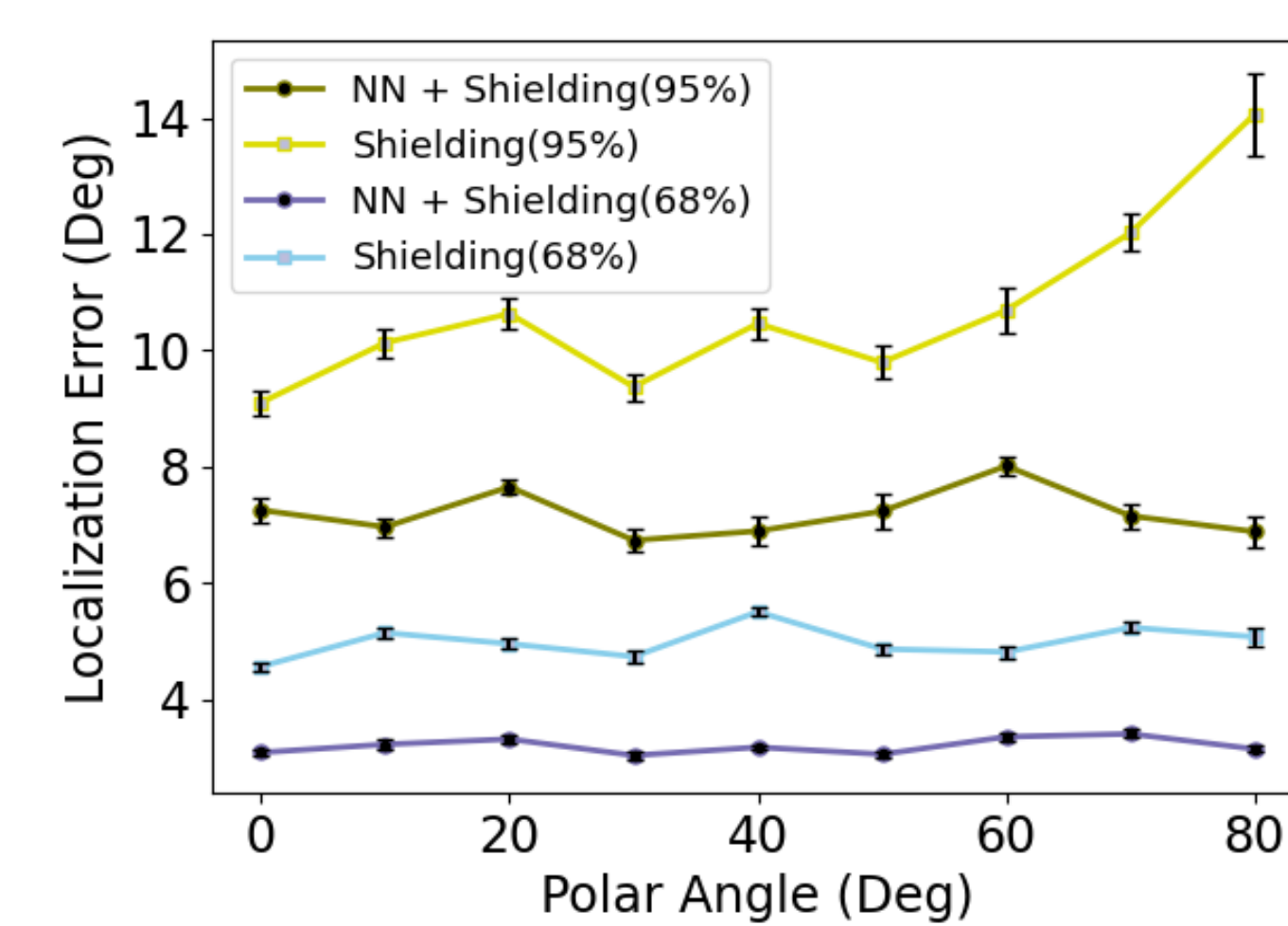
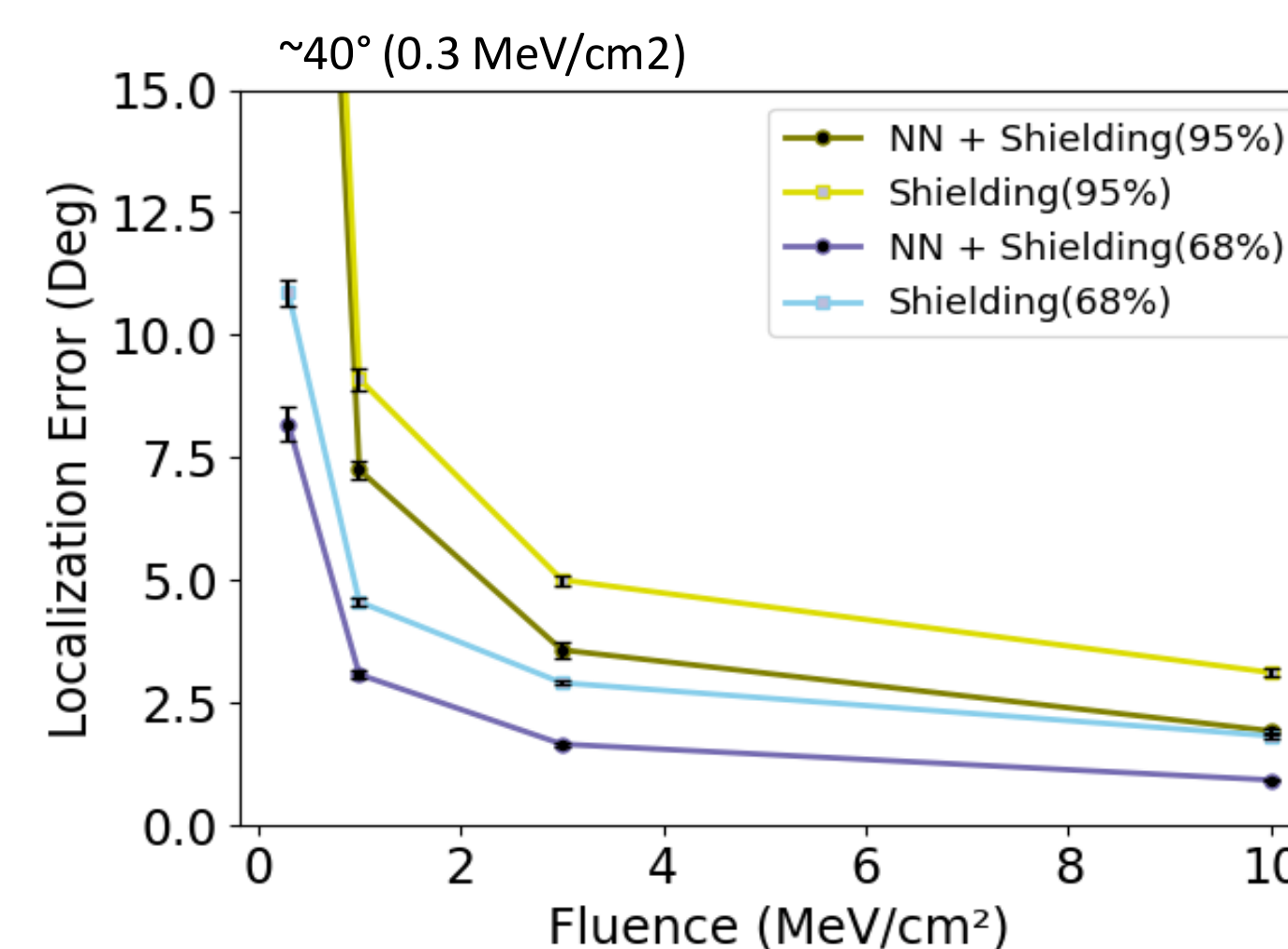
### Multiplexing

- Power and weight budget means 3-to-1 passive multiplexing of WLS SiPMs into single SMART preamp channel
- **Solution:** different index of refraction in silicon epoxy at tile interfaces causes optical light piping down rows of tiles.
- Position/energy reconstruction is three stage process:
  1. Use individual edge detector outputs to guess which of 3 fibers
  2. Perform centroiding based on fiber positions
  3. Use inferred position to look up signal-to-energy conversion from edge detector

5

## Localization Accuracy (ADAPT)

- Tested performance at incident polar angles ( $0^\circ$ - $80^\circ$ ) with  $45^\circ$  azimuthal angles
- New application of a neural network (MLP) motivated by [10]. Enhanced initial estimates of the errors in the inferred angle by updating the weights applied to the circles in the iterative least-squares refinement stage
- For a normal burst, at fluences above  $1 \text{ MeV}/\text{cm}^2$ , accuracy below  $5^\circ$ , 68% of the time
- At  $1 \text{ MeV}/\text{cm}^2$ , accuracy within  $5$ - $6^\circ$  68% of the time for bursts well above the horizon ( $\leq 60^\circ$ )



6

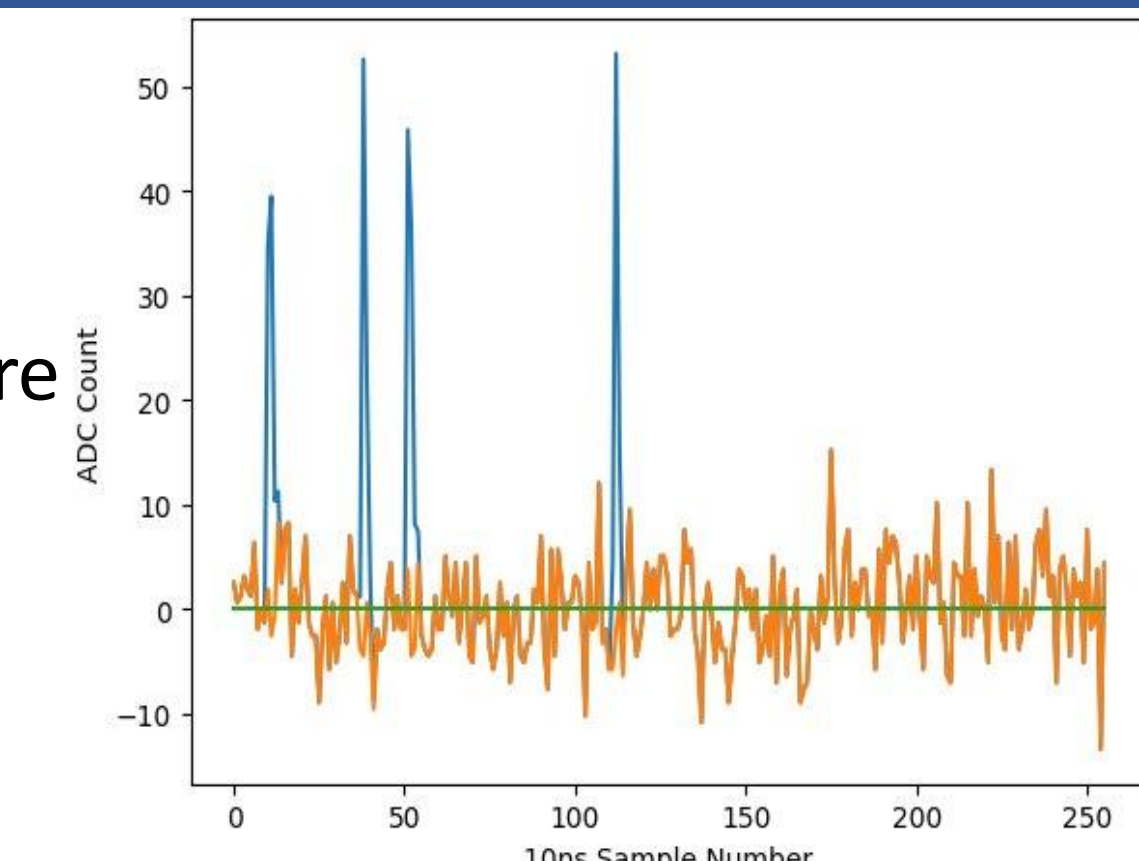
### Zero Suppression

- ALPHA ASICs use an external global trigger
- For a Compton event, a small number of WLS fibers capture optical photons, but all channels are read out
- We can potentially zero-suppress by identifying single-PE impulse response signal spikes in the time domain.

### Background and Pileup

- Apply thresholding in the earlier parts of the pipeline to deal with background events

**Neural Network:** Current model was trained only on earlier simulations without multiplexing, background or pileup. We plan to incorporate updated simulations and train a new model



[1] J. Buckley et al., The Advanced Particle-Astrophysics Telescope (APT) Project Status, in Proc. of 37th International Cosmic Ray Conference, vol. 395, pp. 655:1–655:9, July 2021, DOI.  
 [2] M. Sudvar et al., A Fast GRB Source Localization Pipeline for the Advanced Particle-Astrophysics Telescope, in Proc. of 37th International Cosmic Ray Conference, vol. 395, pp. 588:1–588:9, July 2021, DOI.  
 [3] W. Chen et al., The Advanced Particle-Astrophysics Telescope: Simulation of the Instrument Performance for Gamma-Ray Detection, in Proc. of 37th Int'l Cosmic Ray Conference, vol. 395, pp. 590:1–590:9, 2021, DOI.  
 [4] S. Agostinelli, J. Allison, K. Amako et al., Geant4 — a simulation toolkit, Nuclear Instruments and Methods in Physics Research Section A: Accelerators, Spectrometers, Detectors and Associated Equipment 506 (2003) 250.  
 [5] M. Sudvar et al., Front-End Computational Modeling and Design for the Antarctic Demonstrator for the Advanced Particle-Astrophysics Telescope. Poster PGA1-09 (physical).  
 [6] W. Chen, J. Buckley et al., Simulation of the instrument performance of the Antarctic Demonstrator for the Advanced Particle-Astrophysics Telescope in the presence of the MeV background. Poster PGA0-22 (online).  
 [7] S. Boggs and P. Jean, Event reconstruction in high resolution Compton telescopes, Astronomy and Astrophysics Supplement Series 145 (2000) 311.  
 [8] D. Band et al., BATSE observations of gamma-ray burst spectra. I. spectral diversity, Astrophys. J. 413 (1993) 281.  
 [9] "Overview of the Fermi GBM." [https://fermi.gsfc.nasa.gov/ssc/data/analysis/documentation/Cicerone/Cicerone\\_Introduction/GBM\\_overview.html](https://fermi.gsfc.nasa.gov/ssc/data/analysis/documentation/Cicerone/Cicerone_Introduction/GBM_overview.html), Jan. 2020.  
 [10] S. Takashima, H. Odaka, H. Yoneda, Y. Ichinohe, A. Bamba, T. Aramaki et al., Event reconstruction of compton telescopes using a multi-task neural network, Nuclear Instruments and Methods in Physics Research Section A: Accelerators, Spectrometers, Detectors and Associated Equipment 1038 (2022) 166897.